Catal Lett (2007) 117:18–24
DOI 10.1007/s10562-007-9151-4

# Controlling Reaction Pathways for Alcohol Dehydration and Dehydrogenation over FeSBA-15 Catalysts

**Yejun Guan · Ying Li · Rutger A. van Santen · Emiel J. M. Hensen · Can Li**

Received: 15 June 2007 / Accepted: 1 July 2007 / Published online: 17 July 2007


**Abstract** The iron location in FeSBA-15 strongly influences the selectivity to dehydrogenation and dehydration in ethanol conversion. At low iron loading, Fe is present as isolated $Fe^{3+}$ species in the amorphous silica phase. At higher loading additional aggregated forms of iron oxide exist. Isolated $Fe^{3+}$ species in the silica matrix imply Brønsted acidity resulting in selective formation of ethylene, whereas $FeO_x$ clusters catalyze formation of ethylene and aldehyde.

**Keywords** SBA-15 · Iron · Ethanol · Dehydrogenation · Dehydration

## 1 Introduction

In recent times, biomass utilization has been receiving increasing attention due to the need to reduce greenhouse gases and concerns about the dependence on petroleum feedstocks for energy supply. Much is expected from a partial shift to biomass-derived ethanol to reduce carbon dioxide emissions [1, 2]. Recently, considerable developments have been reported in the use of ethanol and ethanol-based oxygenates as alternative motor vehicle fuels, fuel additives [3] or as a feedstock to produce hydrogen [4, 5]. On the other hand, there is also growing interest in converting ethanol to acetaldehyde and ethylene because these are important starting chemicals for the chemicals industry [6, 7]. Dehydration of ethanol to ethylene is preferably carried out over solid acids such as pentasil zeolites [8, 9]. For commercial dehydrogenation to acetaldehyde supported copper and palladium or basic oxides such as magnesium oxide are employed [10–13]. On the other hand, both processes occur also over some transition metal oxides such as ZnO, $Fe_2O_3$ and $Mn_2O_3$ and the selectivity depends on the surface acid-base properties of the oxide [14, 15].

Silica dehydrated at 1,023 K has been reported to partake in ethanol dehydrogenation due to the existence of Si–O–Si or $Si–O^-$ entities [16–18]. Mesoporous materials such as those of the SBA-*n* or M41S families offer opportunities for well-tailored, improved access to their well-defined pores which are larger than those typically found in zeolites [19] Further functionalizaton of the silica surface can be brought about by incorporation of isolated metal ions or small metal oxide clusters [20]. For example, iron-containing mesoporous materials have been reported to show good catalytic performance in vapor-phase *t*-butylation of phenol, liquid-phase benzylation of benzene by benzyl chloride and decomposition of isopropanol [21–24].

Here, we report the application of FeSBA-15 mesoporous materials for the conversion of ethanol to ethylene and

Y. Guan · C. Li (✉)
State Key Laboratory of Catalysis, Dalian Institute of Chemical Physics, Chinese Academy of Sciences, Zhongshan Road 457, Dalian, China
e-mail: canli@dicp.ac.cn

Y. Guan
e-mail: yjguancatal@hotmail.com

Y. Li · R. A. van Santen · E. J. M. Hensen (✉)
Schuit Institute of Catalysis, Eindhoven University of Technology, P.O. Box 513, Eindhoven 5600 MB, The Netherlands
e-mail: e.j.m.hensen@tue.nl

Y. Li
e-mail: ying.li@tue.nl

R. A. van Santen
e-mail: r.a.v.santen@tue.nl

acetaldehyde. We will show that isolated Fe species embedded in the amorphous silica framework of SBA-15 give this mesoporous material typical Brønsted acidic properties, whereas stabilization of small iron oxide clusters confined in the mesopores have weak Lewis acidic and basic functionalities. The former catalyzes the formation of ethylene from ethanol selectively, while the latter produces both ethylene and acetaldehyde from ethanol.

## 2 Experimental

### 2.1 Materials

FeSBA-15 catalysts with a range of Fe loadings were synthesized by a direct synthesis method [25] using tetramethyl orthosilicate (TMOS) and iron nitrate ($Fe(NO_3)_3 \cdot 9H_2O$) as silicon and iron precursors, respectively. The non-ionic triblock copolymer surfactant $EO_{20}PO_{70}EO_{20}$ (P123) was applied as the structure-directing agent. Micellar arrays of this surfactant were stabilized in concentrated hydrochloric acid. In a typical synthesis, 2 g of P123 was dissolved in 70 mL of HCl solution at pH value of 1.5 (solution A). TMOS (3.2 mL) and a certain amount of iron nitrate were mixed with 5 mL of deionized water to get solution B. Solution B was stirred at room temperature for about 10 min to obtain a clear solution, which was subsequently added dropwise to solution A. The mixture of solution A and B was stirred vigorously for 20 h at 313 K and then transferred into an autoclave and aged for 24 h at 373 K. The resulting solid was filtered, washed, and dried at 333 K and calcined at 773 K for 10 h. For comparison, an SBA-15 catalyst without iron species was also prepared [26]. Catalysts are denoted by FeSBA-15(x) where x represents the Fe loading in wt.%.

### 2.2 Catalyst Characterizations

The elemental concentration of Fe was determined by ICP-OES after the sample was dissolved in a mixture of HF and $HNO_3$ . The nitrogen sorption experiments were performed at 77 K on a Micromeretics Tristar system in static measurement mode. Catalyst samples were outgassed at 423 K for 3 h prior to measurement of nitrogen sorption. Pore size distribution curves were calculated from the analysis of desorption branch of the isotherm by the BJH (Barrett-Joyner-Halenda) method. TEM images were acquired on a FEI Tecnai 20 at an acceleration voltage of 200 kV. Typically, a small amount of catalyst was suspended in ethanol, sonicated and dispersed over a Cu grid with a carbon film. Infrared spectra of adsorbed pyridine were taken on a Thermo Nicolet NEXUS 470 FT-IR spectrometer. The samples were pressed into self-supporting wafers and were evacuated in a vacuum cell at 673 K for 2 h. Background spectra were recorded after the sample was cooled to room temperature. Pyridine was then admitted to the cell and the infrared spectra of adsorbed pyridine were recorded after degassing at 423 K. Diffuse reflectance UV–vis reflection spectra were recorded at ambient temperature on a Shimadzu UV-2401 with a 60-mm integration sphere. $BaSO_4$ was used as reference material.

### 2.3 Conversion of Ethanol

Reaction data were collected in an atmospheric-pressure quartz plug flow reactor. Typically, 50 mg of catalyst diluted with a proper amount of SiC to ensure isothermal plug flow conditions was contained between two quartz wool plugs. Gases were delivered by Brooks thermal mass flow controllers. Ethanol was fed by a Bronkhorst liquid mass flow controller and controlled evaporator mixer. The feed mixture consisted of 2 vol.% ethanol in He (in some cases 2 vol.% $O_2$ was added) at a total flow rate of $100\,ml \cdot min^{-1}$ . The reaction effluent was analyzed by a combination of a Hewlett-Packard 5890 gas chromatograph (FID, HP-5 column) and a mass spectrometer (Balzers TPG-310).

## 3 Results and Discussion

### 3.1 Characterization

The nitrogen sorption isotherms of Fe-containing catalysts are collected in Fig. 1. The isotherms of SBA-15 and FeSBA-15(0.3) are typical for mesoporous SBA-15, which exhibits a two-dimensional *P6mm* structure with open cylindrical mesopores having uniform diameters of about 6 nm. The isotherms of the catalysts with a higher Fe loading display a one-step capillary condensation and a two-step desorption branch. The one-step capillary condensation indicates that these materials have uniform mesopores. A two-step desorption branch has been reported before by Voort et al. [27] for SBA-15. These authors proposed that cylindrical mesopores are plugged by amorphous silica particles that are created by a large excess of the silica source used in the synthesis and by rapid hydrolysis of the silicon alkoxide at very low pH. In the present case, high Fe loadings were employed and likely the plugging of mesopores derives from iron oxide particles about 3–5 nm blocking the mesopores as shown in Fig. 2. It might be expected that at high Fe loadings due to extensive pore blocking part of the mesopore surface area

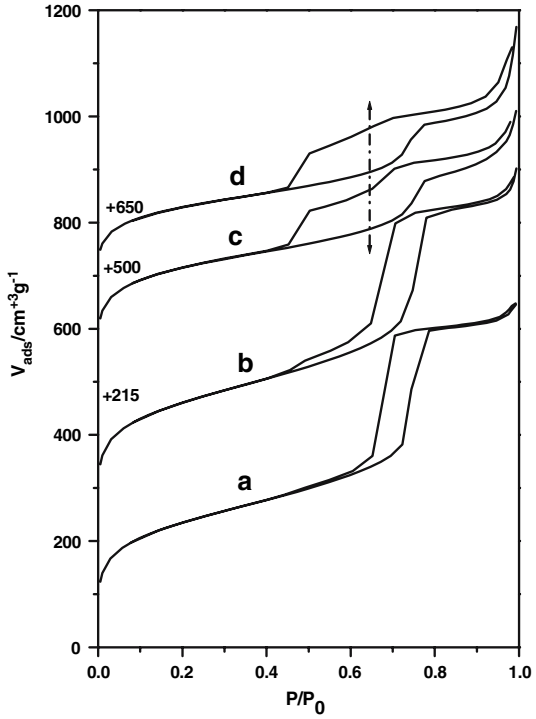


**Fig. 1** BET adsorption-desorption curves of (**a**) SBA-15; (**b**) FeSBA-15(0.3); (**c**) FeSBA-15(4); (**d**) FeSBA-15(14)

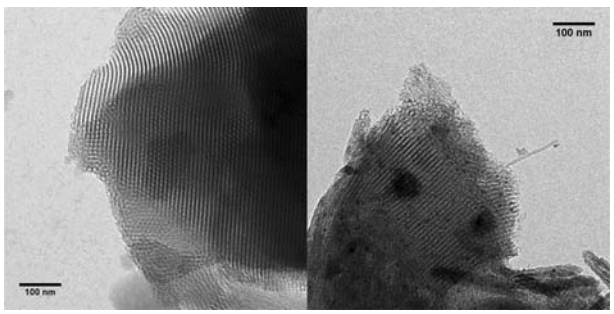


**Fig. 2** Representative TEM images of SBA-15 (left) FeSBA-15(14) (right)

is not accessible anymore to the reractants. As expected, the SBA-15 material exhibited a single desorption step.

Figure 3 shows the UV–visible spectra of the calcined FeSBA-15(x) catalysts. The UV–visible spectra of FeSBA-15(0.3) has one strong absorption band centered around 257 nm. With increasing iron loading, strong bands at 367 and 530 nm are observed. Li et al. [25] have systematically investigated the correlations between the absorption bands and the Fe loadings of FeSBA-15 materials prepared by a similar method. The single absorption band between 210 nm and 250 nm was attributed to isolated four-coordinated $Fe^{3+}$ ions. This band is associated with the ligand to metal charge transfer of $t_1 \rightarrow t_2$ and $t_1 \rightarrow e_g$ transitions involving isolated four-coordinated $Fe^{3+}$ in $[FeO_4]^-$ tetrahedra. In our case, the absorption band centered around 257 nm. Hensen et al. [28] have observed the absorption of isolated $Fe^{3+}$ slightly shift to higher wavelength in Fe-MFI materials, which may be interpreted in terms of an increased number of oxygen ligands resulting from partial $Fe^{3+}$ migration from framework to extraframework positions. The isolated octahedral extraframework $Fe^{3+}$ has a characteristic band of 280 nm. Thus, framework and extraframework isolated $Fe^{3+}$ are simultaneously present in FeSBA-15(0.3). Vinu et al. [21–23] also reported an absorption band at 265 nm which was assigned to isolated $Fe^{3+}$ species in Fe-containing SBA-1 and SBA-15. At higher Fe loadings, additional absorption bands at 367 nm and 530 nm suggest the formation of iron oxide clusters of various degree of agglomeration in the mesopores.

## 3.2 Catalytic Conversion of Ethanol to Acetaldehyde and Ethylene

### *3.2.1 Reactions in the Absence of* $O_2$

Figure 4a displays the ethanol conversion as a function of reaction temperature for the SBA-15 and FeSBA-15(x) catalysts in the absence of oxygen. Siliceous SBA-15 shows 10% ethanol conversion at 673 K with selectivities to acetaldehyde and ethylene both being 30%. FeSBA-15(x) catalysts displays a much higher catalytic activity than siliceous SBA-15. For instance, the presence of 0.3 wt.% Fe in FeSBA-15(0.3) results in a strong increase of the conversion (68%) at 673 K. A further increase of the iron loading from 0.3 wt.% to 14 wt.% results in an increase of ethanol conversion from 29% to 49% at 623 K.

Figure 4b and c show the selectivities to acetaldehyde and ethylene as a function of reaction temperature and Fe loading. The selectivity to acetaldehyde for siliceous SBA-15 is 30% above 573 K. In this temperature range, the acetaldehyde selectivity increases strongly with iron loading. The acetaldehyde selectivity is the lowest for FeSBA-15(0.3) and the highest for FeSBA-15(14) at 623 K. An opposite trend is observed for the ethylene selectivity (Fig. 4c). The selectivity to ethylene is 40% at 673 K for siliceous SBA-15, whereas it increases strongly upon iron incorporation for FeSBA-15(0.3). At 623 K, the ethylene selectivity decreases from 82% for FeSBA-15(0.3) to 60% and 44% for FeSBA-15(4) and FeSBA-15(14), respectively. Over bulk iron oxide, the ethylene selectivity is 31%. These results indicate that the strongly varying Fe speciation in FeSBA-15(x) affects the rates of dehydrogenation and dehydration of ethanol.

Table 1 lists the yield of ethylene and acetaldehyde over SBA-15 and FeSBA-15(x). The yields of ethylene and acetaldehyde over SBA-15 are 3.9% and 3.3%, respectively. The low yield is due to the weak acid-base

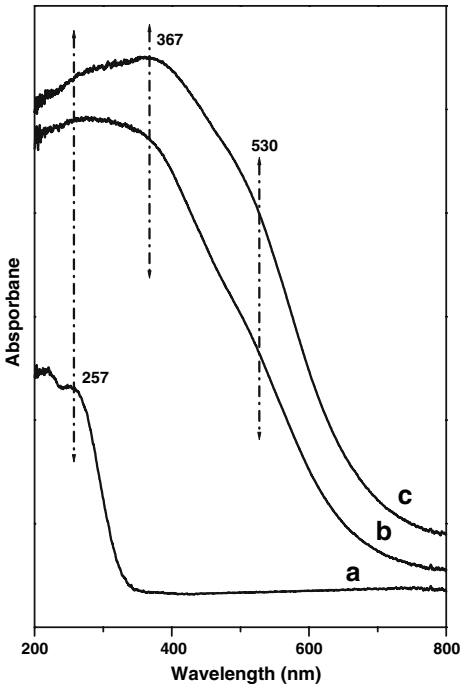


**Fig. 3** UV–vis of FeSBA-15 with different iron loadings: (**a**) FeSBA-15(0.3); (**b**) FeSBA-15(4); (**c**) FeSBA-15(14)

properties of the silica surface. Upon incorporation of isolated $Fe^{3+}$ ions in the silica, the ethylene yield increases strongly whereas the acetaldehyde yield does not change. The increased ethylene yield is associated with the appearance of Brønsted acidity due to the replacement of tetravalent Si by trivalent Fe (Scheme 1). Figure 5 displays the spectra of pyridine adsorbed to siliceous SBA-15 and FeSBA-15(0.3). The spectra only show pyridine hydrogen-bonded to the surface. These bands are much more pronounced in FeSBA-15 than in SBA-15. The relatively weak acidity of these hydroxyl groups associated with framework Fe prevents protonation of pyridine and hence the corresponding characteristic bands at 1,547 and 1,640 $cm^{-1}$ are not observed. Recently, it was found that well-prepared AlSBA-15 has a higher acidity enabling protonation of pyridine [29]. We propose that the weakly Brønsted acid sites promote the dehydration of ethanol to ethylene. They do not further influence the dehydrogenation route. This tallies with the notion that dehydrogenation is catalyzed by Si–O–Si sites of the SBA-15 surface [16, 17]. Clearly, these sites are not affected by the presence of a small amount of Fe embedded in silica. Such isolated $Fe^{3+}$ species that lead to the presence of Brønsted acid reaction sites

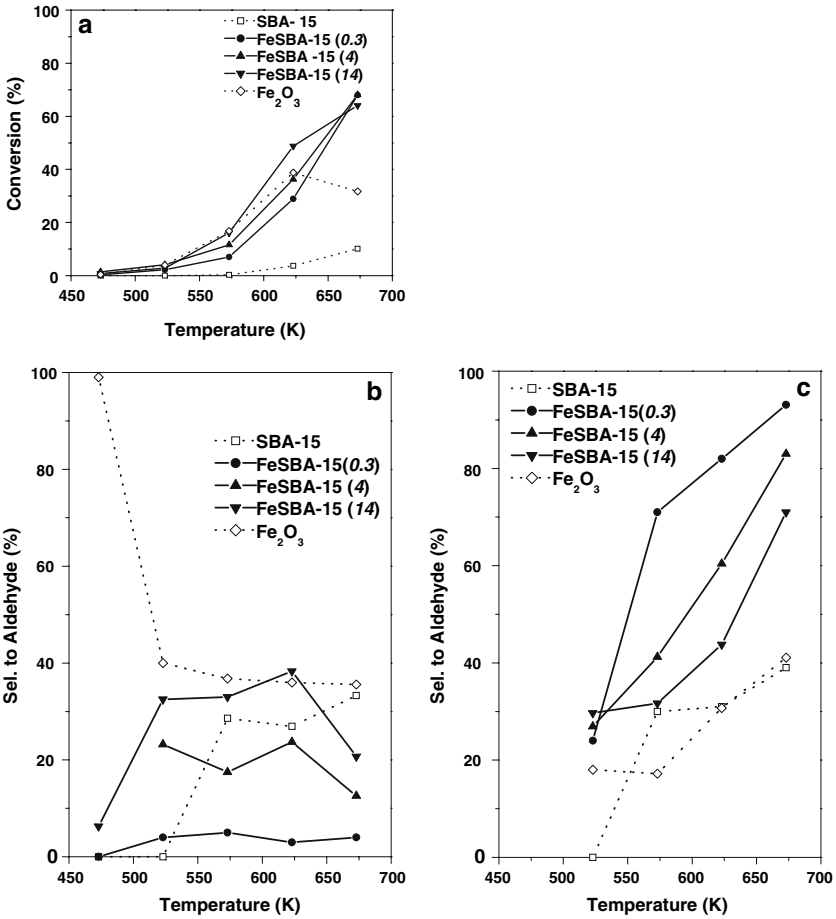


**Fig. 4** FeSBA-15(x) and SBA-15 materials for the ethanol conversion in the absence of $O_2$ : (**a**) conversion of ethanol vs. reaction temperature; (**b**) selectivity to acetaldehyde vs. reaction temperature and (**c**) selectivity to ethylene vs. reaction temperature

**Table 1** Physical parameters of FeSBA-15(x) and products distribution at 673 K

| Fe Loading (wt.%) | UV–vis (nm) | $SA_{BET}$ ($cm^2/g$) | $Yield_{max}$ (without $O_2$) | | $Yield_{max}$ (with $O_2$) | |
|---|---|---|---|---|---|---|
| | | | Ethylene (%) | Acetaldehyde (%) | Ethylene (%) | Acetaldehyde (%) |
| 0 | – | 780 | 3.9 | 3.3 | 5.5 | 24.6 |
| 0.3 | 257 | 875 | 63.3 | 2.7 | 44.9 | 24.5 |
| 4 | 367, 530 | 760 | 56.5 | 8.5 | 19.1[a] | 38.4[a] |
| 14 | 367, 530 | 634 | 45.5 | 13.3 | 9[a] | 33[a] |
| 100 | – | 12 | 11.9[a] | 13.9[a] | 6.2[a] | 28[a] |

[a] 623 K

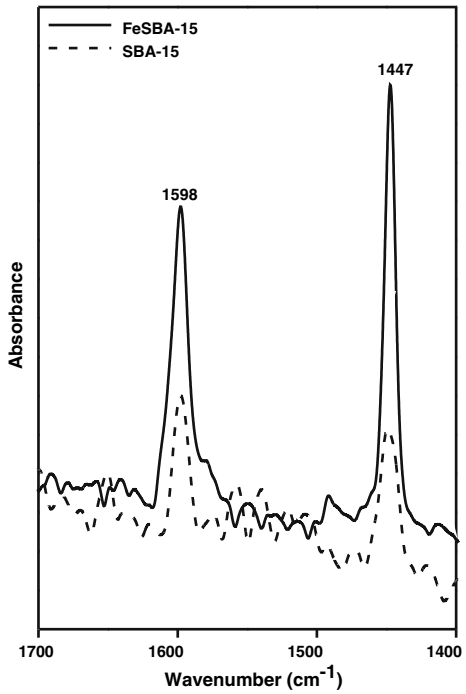


**Fig. 5** Infrared spectra of pyridine adsorbed to SBA-15 and FeSBA-15(0.3) after outgassing at 423 K

have also been reported to be active for benzylation of benzene and other aromatics using benzyl chloride [22, 23] and the dehydration of propanol [24, 30]. Agglomerated iron oxide clusters in the mesopores of FeSBA-15(4) increase the acetaldehyde yield from 2.7% to 8.5%. A further increase of the Fe loading to 14% increases the yield further to 13.9%, which is similar to the yield over pure $Fe_2O_3$ (13.3%). This forms an indication that the properties of the iron oxide particles approximate those of bulk $Fe_2O_3$ . However, the yield of ethylene (45.5%) over FeSBA-15(14) is considerably higher than over pure $Fe_2O_3$ (11.9%) and this may be related to the presence of a higher number of Brønsted acid sites that catalyze the dehydration pathway.

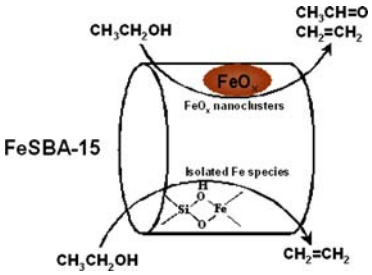


**Scheme 1** Proposed mechanism for ethanol conversion over FeSBA-15(x)

### 3.2.2 *Reactions in the Presence of* $O_2$

The catalytic performance of ethanol conversion in the presence of molecular oxygen (2 vol.%) as a function of reaction temperature and Fe loading is displayed in Fig. 6a. Ethanol conversion over SBA-15 is 55 % at 673 K with an acetaldehyde selectivity of 45 % (Fig. 6b) and an ethylene selectivity of 11 % (Fig. 6c), the remaining products being total combustion products. The yield of acetaldehyde (25 %) in the presence of oxygen is much higher than in its absence (3.3 %), while the ethylene yield remains almost similar (Table 1). For the iron-containing catalysts, the presence of oxygen in the reactant feed increases the yield to acetaldehyde while decreasing the yield to ethylene. These findings show that oxygen promote the dehydrogenation pathway. Indeed, addition of oxygen was found to increase the rate constant of dehydrogenation reaction over silica as reported by Yao et al. [31]. This explanation may also apply to the effect of oxygen addition to FeSBA-15(0.3). By incorporation of isolated $Fe^{3+}$ species, the conversion of ethanol increases to 91% at 673 K, with selectivities to acetaldehyde and ethylene of 27% and 50%, respectively. The yield of acetaldehyde is 25%, which is equal to the siliceous SBA-15, while the yield of ethylene

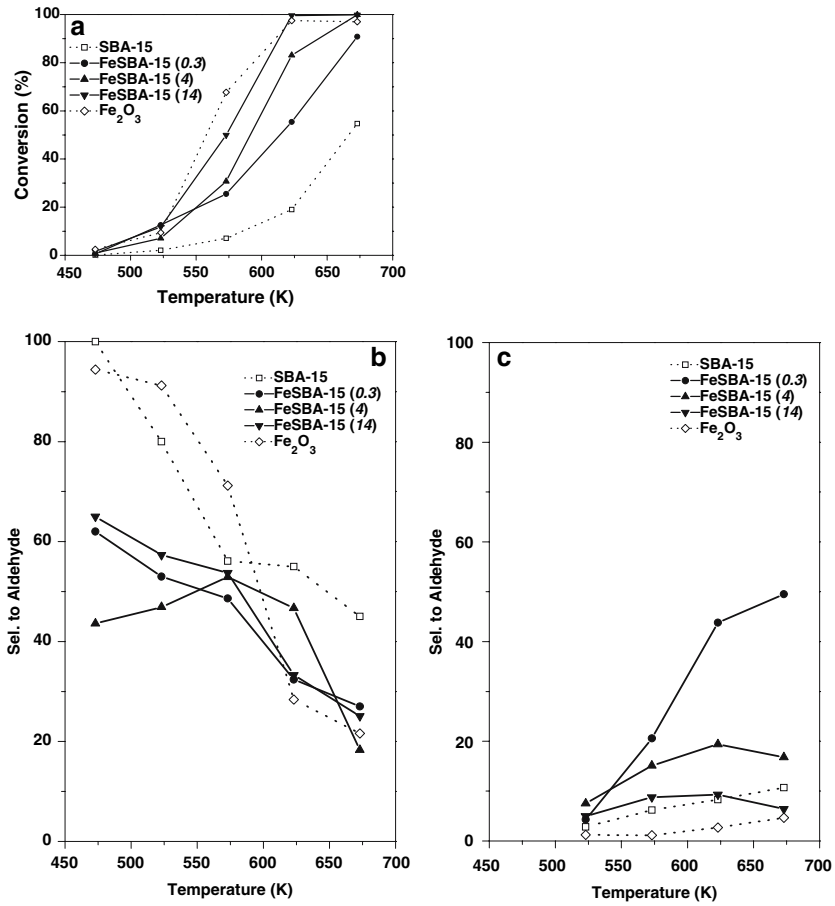


**Fig. 6** FeSBA-15(x) and SBA-15 materials for the ethanol conversion in the presence of $O_2$ : (**a**) conversion of ethanol vs. reaction temperature; (**b**) selectivity to acetaldehyde vs. reaction temperature and (**c**) selectivity to ethylene vs. reaction temperature

is 45%. Meanwhile, the total yields of $C_2$ compounds (69%) remains unchanged compared with that (66%) in the absence of oxygen, which suggest that the oxygen does only change the selectivity of dehydrogenation versus dehydration.

Further increases of Fe loading result in two changes. Firstly, the ratio between yield of acetaldehyde and ethylene $(Y_{acetaldehyde}/Y_{ethylene})$ increases with iron loading, which is related to the formation of $FeO_x$ clusters. Formation of acetaldehyde is related to the surface basic or redox active sites of small $FeO_x$ clusters. Furthermore, the values of $Y_{acetaldehyde}/Y_{ethylene}$ in the presence of oxygen are much higher than those in the absence of oxygen. Bowker et al. [32] have reported that dehydration occurs at anion vacancies (Lewis acid sites) over metal oxides, whilst dehydrogenation is catalyzed by stoichiometric sites (Lewis basic sites). The concentration of surface anion vacancies is dependent on the reduction degree of oxide. Thus, the number of dehydration sites should be higher in the absence of oxygen, whereas the number of dehydrogenation sites increase upon oxygen addition. The oxygen adatoms may also play a role in the reductive elimination of adsorbed ethoxy species to acetaldehyde via water formation. Secondly, the total yield of $C_2$ products (ethylene and acetaldehyde) decreases with increasing iron loading, which is attributed to the total oxidation activity of the iron oxide phase at higher temperatures. It is interesting to note that FeSBA-15(4) shows higher selectivity to acetaldehyde than FeSBA-15(0.3) and FeSBA-15(14) at 623 K with an acetaldehyde yield of 38%. These results indicate that by tuning the Fe loading in the SBA-15 materials and controlling the oxygen content in the feed, one may selectively convert ethanol to ethylene or acetaldehyde with desired conversion and selectivity.

## 4 Conclusion

FeSBA-15 materials were synthesized by a direct hydrothermal method. UV–vis absorption band at 256 nm indicates the Fe species exist mainly as isolated $Fe^{3+}$ incorporated in the amorphous silica phase at low Fe loading, and the absorption bands at 367 and 530 nm suggest $FeO_x$ cluster are formed at high Fe loadings. Isolated $Fe^{3+}$ species in the siliceous surface generate sufficiently strong Brønsted acidity to dehydrate ethanol to ethylene, with maximum ethylene yields of 63% in the absence and 45% in the presence of oxygen at 673 K.

Small $FeO_x$ clusters show both dehydration and dehydrogenation activity. The presence of oxygen promotes the rate of dehydrogenation reaction pathway over these catalysts. The yield of ethylene and acetaldehyde depends on the iron loading and the oxygen content in the reactant feed. FeSBA-15(4) shows the highest catalytic activity to acetaldehyde, which gives acetaldehyde yield of 39% at 623 K in the presence of oxygen. Higher amounts of $FeO_x$ clusters result in increased contribution of total oxidation products and very low $C_2$ hydrocarbon product yields.

**Acknowledgments** This work was financially supported by Program for Strategic Scientific Alliances between China and Netherlands funded by the Royal Netherlands Academy of Arts and Science (Grant No. 04-PSA-M-01) and the Chinese Ministry of Science and Technology (Grant No. 2004CB720607).

## References

1. Bridgwater T (2006) J Sci Food Agric 86:1755
2. Huber GW, Iborra S, Corma A (2006) Chem Rev 106:4044
3. Niven RK (2005) Renew Sustain Energ Rev 9:535
4. Gucbilmez Y, Dogu T, Balci S (2006) Ind Eng Chem Res 45:3496
5. Haryanto A, Fernando S, Murali N, Adhikari S (2005) Energy Fuels 19:2098
6. Mallat T, Baiker A (2004) Chem Rev 104:3037
7. Gucbilmez Y, Dogu T (2006) Ind Eng Chem Res 45:3496
8. Phillips CB, Datta R (1997) Ind Eng Chem Res 36:4466
9. Kondo JN, Ito K, Yoda E, Wakabayashi F, Domen K (2005) J Phys Chem B 109:10969
10. Rioux RM, Vannice MA (2003) J Catal 216:362
11. Chang F-W, Kuo W-Y, Lee K-C (2003) Appl Catal A 246:253
12. Issaadi R, Garin F, Chitour C (2006) Catal Today 113:166
13. Takezawa N, Hanamaki C, Kobayashi H (1975) J Catal 38:101
14. Vohs JM, Barteau MA (1989) Surf Sci 221:590
15. Zaki T (2005) J Colloid Interface Sci 284:606
16. Matsumura Y, Hashimoto K, Yoshida S, J Chem Soc Chem Commun (1987) 1599
17. Matsumura Y, Hashimoto K, Yoshida S (1989) J Catal 117:135
18. Fleisher M, Stonkus V, Leite L, Lukevics E (2004) Int J Quant Chem 100:407
19. Taguchi A, Schuth F (2005) Micropor Mesopor Mater 77:1
20. Vinu A, Hossain KZ, Sriga K (2005) J Nanosci Nanotech 5:347
21. Vinu A, Krithiga T, Murugesan V, Hartmann M (2004) Adv Mater 16:1817
22. Vinu A, Sawant DP, Ariga K, Hossain KZ, Halligudi SB, Hartmann M, Nomura M (2005) Chem Mater 17:5339
23. Vinu A, Krithiga T, Balasubramanian VV, Asthana A, Srinivasu P, Mori T, Ariga K, Ramanath G, Ganesan PG (2006) J Phys Chem B 110:11924
24. Trejda M, Ziolek M (2005) Catal Today 101:109
25. Li Y, Feng ZC, Lian YX, Sun KQ, Zhang L, Jia GQ, Yang QH, Li C (2005) Micropor Mesopor Mater 84:41
26. Zhao DY, Feng JL, Huo QS, Melosh N, Fredrickson GH, Chmelka BF, Stucky GD (1998) Science 279:548
27. Van Der Voort P, Ravikovitch PI, De Jong KP, Benjelloun M, Van Bavel E, Janssen AH, Neimark AV, Weckhuysen BM, Vansant EF (2002) J Phys Chem B 106:5873
28. Hensen EJM, Zhu Q, Janssen RAJ, Magusin PCMM, Kooyman PJ, van Santen RA (2005) J Catal 233:123
29. Li Y, Feng Z, Xin H, Tan F, Zhang J, Magusin PCMM, Hensen EJM, van Santen RA, Yang Q, Li C (2006) J Phys Chem B 110:26114
30. Decyk P, Trejda M, Kujawa J, Glaszczka K, Bettahar M, Monteverdi S, Mercy M (2003) J Catal 219:146
31. Yao SL, Yang FO, Shimumora S, Sakurai H, Tabata K, Suzuki E (2000) Appl Catal A 198:43
32. Bowker M, Houghton H, Waugh KC (1982) J Chem Soc Faraday Trans I 78:2573